Despite a Conserved Cystine Knot Motif, Different Cyclotides Have Different Membrane Binding Modes

Conan K. Wang, Michelle L. Colgrave, David C. Ireland, Quentin Kaas, and David J. Craik*
University of Queensland, Institute for Molecular Bioscience, Brisbane, Queensland, Australia

ABSTRACT Cyclotides are cyclic proteins produced by plants for defense against pests. Because of their remarkable stability and diverse bioactivities, they have a range of potential therapeutic applications. The bioactivities of cyclotides are believed to be mediated through membrane interactions. To determine the structural basis for the biological activity of the two major subfamilies of cyclotides, we determined the conformation and orientation of kalata B2 (kB2), a Möbius cyclotide, and cycloviolacin O2 (cO2), a bracelet cyclotide, bound to dodecylphosphocholine micelles, using NMR spectroscopy in the presence and absence of 5- and 16-doxylstearate relaxation probes. Analysis of binding curves using the Langmuir isotherm indicated that cO2 and kB2 have association constants of 7.0×10^3 M^{-1} and 6.0×10^3 M^{-1}, respectively, consistent with the notion that they are bound near the surface, rather than buried deeply within the micelle. This suggestion is supported by the selective broadening of micelle-bound cyclotide NMR signals upon addition of paramagnetic Mn ions. The cyclotides from the different subfamilies exhibited clearly different binding orientations at the micelle surface. Structural analysis of cO2 confirmed that the main element of the secondary structure is a β-hairpin centered in loop 5. A small helical turn is present in loop 3. Analysis of the surface profile of cO2 shows that a hydrophobic patch stretches over loops 2 and 3, in contrast to the hydrophobic patch of kB2, which predominantly involves loops 2 and 5. The different location of the hydrophobic patches in the two cyclotides explains their different binding orientations and provides an insight into the biological activities of cyclotides.

INTRODUCTION

Cyclotides are circular proteins found mainly in Rubiaceae (coffee) and Violaceae (violet) plants, where their natural function is in host defense (1–6). They are characterized by a cyclic cystine knot (CCK) motif consisting of a head-to-tail cyclized backbone and a knotted arrangement of disulfide bonds (1,7). The CCK motif accounts for the remarkable stability of cyclotides under harsh thermal, chemical, and enzymatic conditions (8). The amino acid residues between successive Cys residues form backbone loops that project from the compact CCK core, and variations in these residues are responsible for the range of bioactivities of cyclotides, including anti-HIV (4), uterotonic (9), antimicrobial (10), hemolytic (11), cytotoxic (12), neurotensin antagonistic (13), antifouling (14), and pesticidal activities (15–19). The combination of sequence variation, remarkable stability, and diverse bioactivities makes cyclotides attractive as drug scaffolds (20).

Cyclotides are divided into two main subfamilies—the Möbius and bracelet subfamilies—depending on the presence or absence, respectively, of a *cis*-Pro peptide bond in loop 5 (1). The majority (>70%) of cyclotides belong to the bracelet subfamily (6). Fig. 1 illustrates sequence variations between the two subfamilies and highlights their common CCK motif (21). Many of the side chains of hydrophobic residues project outward from the CCK core, which gives rise to surface exposed hydrophobic patches on cyclotides. In bracelet cyclotides, a short helical segment is located in loop 3 and is a major differentiating feature between the two subfamilies.

The plant defense hypothesis for the natural function of cyclotides is based on findings that two Möbius cyclotides, kalata B1 (kB1) and kalata B2 (kB2), inhibit the growth of lepidopteron larvae (15,22). This defense role may explain why cyclotide-bearing plants typically express a large suite of cyclotides. For example, ~20 cyclotides are present in *Oldenlandia affinis* (23), the African herb from which the first cyclotide, kB1, was originally isolated. Cyclotides have also been reported to be toxic to the golden apple snail, which is a major pest of rice crops (18), and to nematode parasites of sheep (17).

It is thought that cyclotides exert their bioactivities through membrane interactions, consistent with their hemolytic, antimicrobial, and cytotoxic activities. An examination of the guts of lepidopteron larvae after consumption of kB1 in artificial diets showed that it induces disruption of the microvilli, blebbing, swelling, and rupture of gut epithelial cells, clearly implicating membrane interactions in the insecticidal action of cyclotides (24). A study of the bracelet cyclotide, cycloviolacin O2 (cO2), using dye-loaded cells and liposomes showed that the disruption of cell membranes plays a crucial role in its cytotoxic effect, and hence established a correlation between membrane interaction and activity (25).

Surface plasmon resonance studies of several cyclotides have shown that they bind to lipid membranes (26). Dodecylphosphocholine (DPC) micelles have been used a membrane mimic for NMR studies. A study using spin labels proposed a binding orientation for the prototypical Möbius cyclotide kB1 to micelles (27). Kalata B7 (kB7),

Submitted January 28, 2009, and accepted for publication June 10, 2009.

*Correspondence: d.craik@imb.uq.edu.au

Editor: Josh Wand.

0006-3495/09/09/1471/11 $2.00

doi: 10.1016/j.bpj.2009.06.032

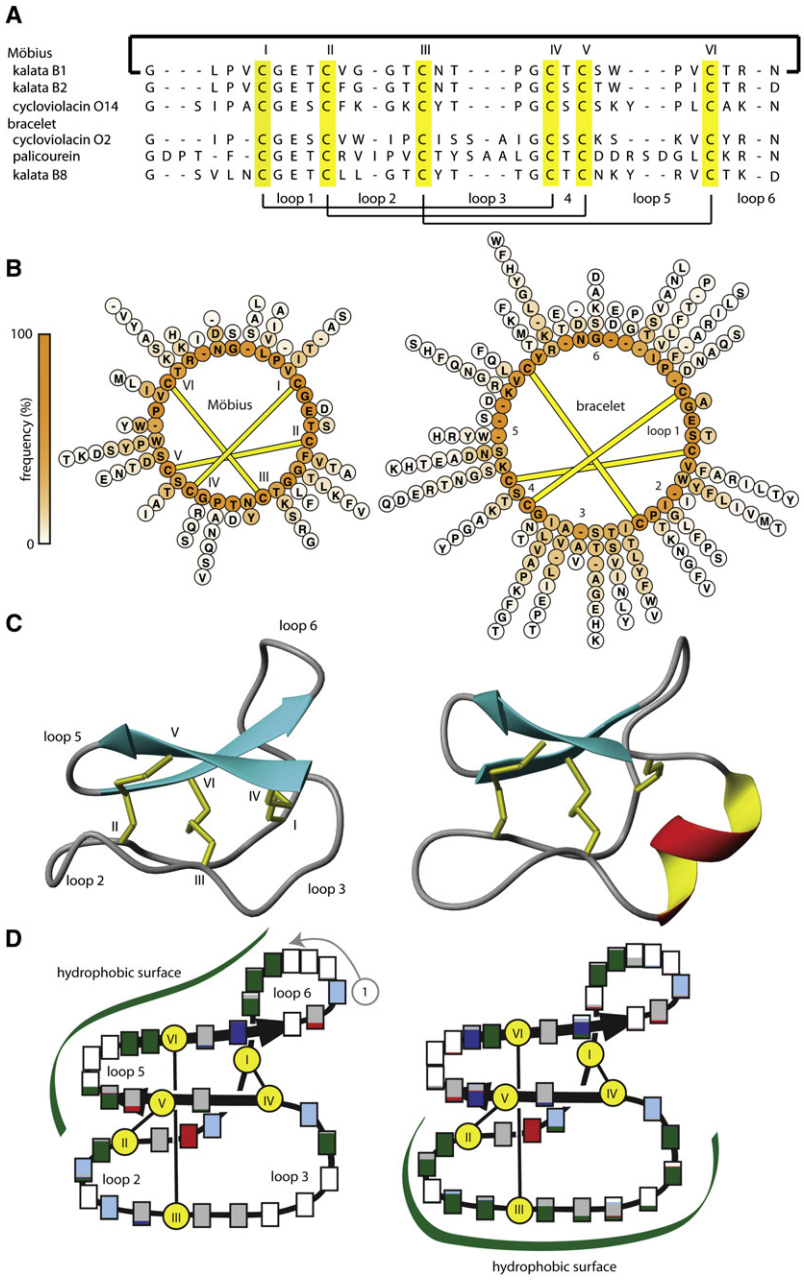

FIGURE 1 Sequence diversity of cyclotides. Panel *A* shows an alignment of selected cyclotide sequences divided into two subfamilies: Möbius and bracelet. The variation in sequences within each subfamily is represented in panel *B*, where the innermost circle shows residues that occur most often. Residue variations protrude outward as spikes. More frequently observed residues have a darker shade. Panel *C* shows kB1 and cycloviolacin (cO1), which belong to the Möbius and bracelet subfamilies, respectively. Panel *D* shows the distribution of residue types in cyclotide sequences for Möbius (*left*) and bracelet (*right*) cyclotides. The distribution of residue types at each position of an alignment, with the same numbering as in panel *A*, is mapped onto the cyclotide framework for Möbius and bracelet cyclotides. A box represents each position of the alignment, with the exception of cysteines, which are shown as yellow circles. Hydrophobic residues are colored green, negatively charged residues are red, positively charged residues are blue, Gly are cyan, and polar residues are gray. Residue types that occur more frequently occupy a larger area in the enclosing box.

another Möbius cyclotide, shows a binding orientation similar to that of kB1 to DPC micelles (28). However, because Möbius and bracelet cyclotides have different loop contents, sizes, and surface profiles, they may also have different modes of membrane binding. Until now, to our knowledge, no binding of bracelet cyclotides to membranes has been reported. The study of bracelet cyclotides is important because they are the most common members of the cyclotide family and are often the most bioactive. For example, the bracelet cyclotide cycloviolacin Y5 is the most potent anti-HIV cyclotide tested so far (29). Here we determined the binding mode of a bracelet cyclotide, cO2, which has potent cytotoxic activity (30), and compared it with the binding of kB2, a Möbius cyclotide with potent insecticidal activity (22). Cycloviolacin O2 has been widely studied for its biological activities and is a representative member of the bracelet subfamily, but its structure has not yet been reported. Our study suggests that although all cyclotides share a conserved CCK motif, they have substantially different orientations of membrane binding.

MATERIALS AND METHODS

Sample preparation and NMR spectroscopy

Using previously described protocols (15), kB2 and cO2 were extracted from *O. affinis* and *Viola odorata*, respectively. Their purity (>95%) was checked by analytical high-performance liquid chromatography and their masses were verified using CyBase, a database of circular proteins (6,31).

NMR analysis also confirmed the purity of the peptides via the absence of any unexplained peaks. NMR samples consisted of various concentrations of kB1 or cO2 in H_2O, D_2O, or DPC (98% deuterium; CIL, Andover, MA). The structure of cO2 was solved for a sample at 1 mM peptide concentration, and the structure of micelle-bound kB2 was solved at 1 mM peptide and 60 mM DPC concentrations. DPC and 5- or 16-doxylstearates (Sigma, St. Louis, MO) were added to samples using aliquots of stock solutions in H_2O and methanol-d4, respectively. The maximum concentration of methanol in the samples was 5%.

NMR spectra were recorded on Avance 500, 600, or 750 MHz spectrometers (Bruker, Karlsruhe, Germany). Two-dimensional (2D) NMR experiments included total correlation spectroscopy (TOCSY) (32) with a 80 ms mixing time, nuclear Overhauser effect spectroscopy (NOESY) (33) with a 200 ms mixing time, and exclusive correlation spectroscopy (E-COSY) (34). Water suppression for the TOCSY and NOESY experiments was achieved by using a modified WATERGATE sequence (35). Spectra were acquired with 4096 data points in the F2 dimension and 512 increments in the F1 dimension. Chemical shifts were referenced to the H_2O solvent signal, which was assigned a chemical shift of 4.65 ppm at 40°C.

Distance restraints were derived from cross-peaks in the NOESY spectra. A summary of the long-range NOEs is provided in the Supporting Material. Spectra were analyzed with SPARKY (36). Backbone dihedral angle restraints were derived from $^3J_{HNH\alpha}$ values measured from peak splitting in a 1D spectrum, and χ^1 dihedral angles were derived from $^3J_{H\alpha H\beta}$ values from the E-COSY spectrum together with NOE intensities. After initial structure calculations were performed with the use of CYANA (37), hydrogen-bond restraints for slowly exchanging amides were added. Final sets of 50 structures were calculated using a torsion angle-simulated annealing protocol within CNS (38). Structures of cO2 were refined in a water shell. The structures were analyzed with MOLMOL (39) and PROCHECK (40), and the 20 lowest-energy structures were deposited in the Protein Data Bank (PDB; ID: 2kcg for cO2 and 2kch for micelle-bound kB2).

Cyclotide binding to DPC micelles

Titration of DPC into kB2 (0.5 mM) and cO2 (2 mM) solutions in 10% D_2O was done at 30°C, pH 2.8. A 1D NMR spectrum and the diffusion rate (41) of the cyclotide-DPC complex were measured at each titration point, ranging from a detergent/peptide ratio of ~2:1 to 60:1 for the kB2 and cO2 samples. In all cases the DPC concentration exceeded the critical micelle concentration. Fast exchange between the unbound and bound states was assumed, which means that the chemical shift of an affected proton (δ_{obs}) depends on the chemical shift of the bound (δ_{bound}) and free (δ_{free}) states, and on the bound peptide and free peptide concentrations according to the following equation:

$$\delta_{obs} = \frac{\delta_{free}[kB1]_{free} + \delta_{bound}[kB1]_{bound}}{[kB1]_0}, \qquad [kB1]_0 = [kB1]_{free} + [kB1]_{bound} \quad (1)$$

The Langmuir isotherm was used for analysis (27) and provided values for K_a (the effective affinity constant of the peptide to the surface of the DPC micelle) and N, the number of DPC molecules that form the site of the peptide binding:

$$\exp\left(\frac{\Delta G^0}{RT}\right) = \frac{1}{K_a} = \frac{[kB1]_{free}\left([DPC] - N[kB1]_{bound}\right)}{N[kB1]_{bound}}. \quad (2)$$

Modeling of the cyclotide-DPC complex

Titration of kB2/DPC or cO2/DPC samples (1 mM peptide) with 5-doxylstearate or 16-doxylstearate was done at 40°C for kB2 and 50°C for cO2. Measurements for cO2 were done at a higher temperature to obtain better-quality spectra. NOESY spectra (100 ms mixing time) were measured at 0 and 8 mM doxylstearate at pH 5 and pH 3 for kB2 and cO2, respectively. The paramagnetic attenuation induced by the doxylstearates was qualitatively characterized by calculating the relative cross-peak intensity (RCI):

$$RCI_i = 100\% \frac{I_i^{probe}}{I_i^0}.$$

Here I_i^{probe} and I_i^0 are the H^N-H^α cross-peak intensities ($H^{\delta 2}$-$H^{\delta 3}$ for prolines) in the spectra of samples with and without a paramagnetic probe.

A model of the cyclotide-micelle complex was built as described previously (42) by constraining atoms to be either inside or outside of a spherical micelle on the basis of their signal attenuation. Using the 5-doxylstearate data, the H^N and H^α atoms for which the relative intensity of their cross-peaks was <20% were restricted to be inside the micelle and other H^N and H^α atoms were restricted to be outside the micelle.

RESULTS

Structural studies of the bracelet cyclotide cO2

To provide a basis for determining the binding mode of cO2 to DPC, the solution structure of cO2 was determined using 2D NMR data. Although amide signals present in the TOCSY spectrum were well dispersed, two amide signals were missing at pH 5 (Ile^{14} and Ser^{15}) and complicated the initial resonance assignment; however, these signals were identified when the pH was lowered to 3. A total of 347 distance restraints, comprising 96 sequential, 109 nonsequential, and 142 intraresidue restraints, were determined from NOESY spectra, and 18 dihedral angle restraints (13 ϕ and five χ^1) were derived using coupling constants from 1D and E-COSY spectra. Slowly exchanging amides were used to derive upper limit distance restraints for six hydrogen bonds. Amide temperature coefficients (see Supporting Material) were used to confirm hydrogen bonds.

Using NOE, dihedral, and hydrogen-bond restraints, a set of 50 structures was calculated by means of torsion angle simulated annealing. A superimposition of the 20 lowest-energy structures obtained after energy minimization is presented in Fig. 2. Most regions of the structure are well defined, with an average root mean-square deviation (RMSD) of 0.35 Å for the backbone atoms and 1.20 Å for all heavy atoms. Structural statistics are summarized in Table 1. Analysis using MOLMOL confirmed that the main element of the secondary structure is a β-hairpin centered in loop 5. A small helical turn is present in loop 3, which is characteristic of bracelet cyclotides. Analysis of the surface profile of cO2 shows that a hydrophobic patch stretches over loops 2 and 3, in contrast to the hydrophobic patch of kB2, which predominantly involves loops 2 and 5.

A pH titration on cO2 (Fig. 2) identified two residues, Ile^{14} and Ser^{15}, whose chemical shifts are most affected by changes in pH. The structure of cO2 shows that the backbone amides for these two residues are involved in a hydrogen-bond network involving the carboxyl of the Glu in loop 1. This hydrogen-bond network has been observed in other cyclotides (e.g., kB1 and cO1) and is believed to help stabilize the cyclotide framework (43).

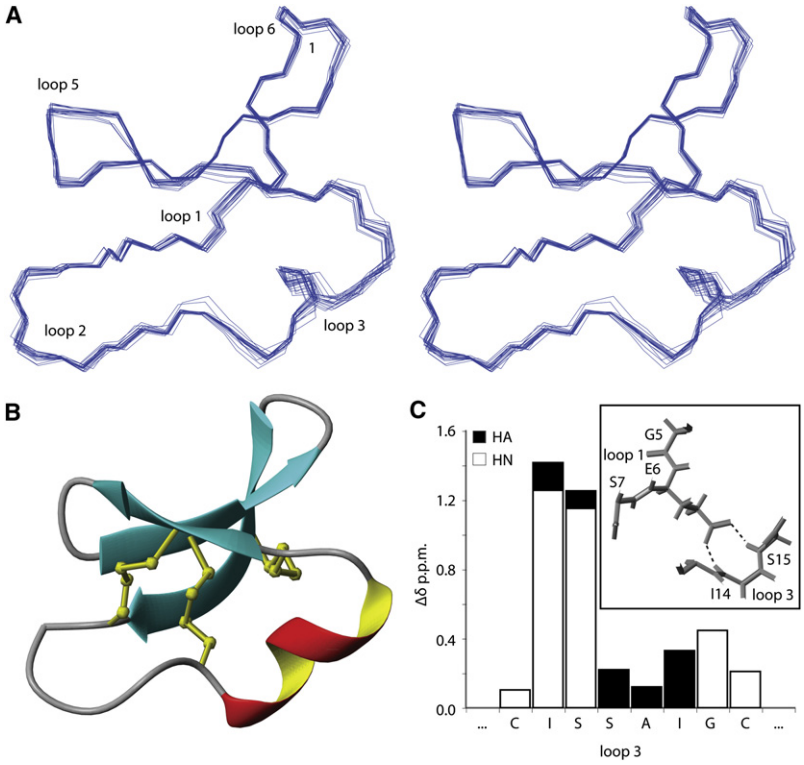

FIGURE 2 Structure of cO2. Panel *A* shows a stereo representation of the solution structure of cO2 solved at pH 5, 30°C. Panel *B* highlights the secondary structure and the disulfide knot. When the pH was varied from 5 to 3, several H^N and H^α chemical shifts changed significantly (>0.1 ppm), as indicated in panel *C*. The two residues having the largest change in H^N chemical shift, Ile^{14} and Ser^{15}, are involved in a hydrogen-bond network with the carboxyl of Glu^6, illustrated in the inset. The large downfield shifts of these two amide signals reflect their hydrogen-bonded status; of interest, however, they mask the diagnostic value of their amide temperature coefficients for defining hydrogen bonds (Supporting Material), a trend that has been reported for peptides in general (51) and cyclotides in particular (52).

Cyclotide-DPC micelle complex

To assess the mode of membrane interaction of cyclotides and hence provide a structural basis for their biological activity, the binding of cO2 and kB2 to DPC micelles was investigated. These peptides were chosen as representative members of the bracelet (cO2) and Möbius (kB2) cyclotide subfamilies because although they have been well characterized in terms of their biological activities, they have not been structurally characterized in the presence of membrane mimics. The chemical shifts of selected protons were monitored as the DPC/peptide mole ratio (D/P) was varied. When the exchange between bound and free peptide species is fast on the NMR chemical-shift timescale, the observed chemical shift of an affected proton depends on the fraction of bound peptide. Fig. 3 shows the changes in chemical shift of the $H^{\varepsilon 1}$ proton of Trp^{10} for cO2 and Trp^{23} of kB2 as a function of D:P. When D/P reached ~40:1 for cO2 and 20:1 for kB2, all of the peptide was micelle-bound. Analysis of the binding curve using the Langmuir isotherm indicated that cO2 and kB2 have effective association constants (K_a) of $7.0 \times 10^3\ M^{-1}$ and $6.0 \times 10^3\ M^{-1}$, respectively. These affinities are consistent with the notion that cO2 and kB2 are bound near the surface, rather than buried deeply within the micelle, and are similar to the result reported recently for kB1 (K_a of $7.9 \times 10^3\ M^{-1}$) (27). Although it is not clear that it is entirely appropriate to discuss peptide-micelle interactions in terms of K_a values, and hence we refer to them as ''effective'' K_a values, the main finding from these studies is that there is a definite association between both subfamilies of cyclotides and DPC micelles.

An analysis of the backbone chemical shifts of the free and bound peptides (Fig. 4) established that different regions of cO2 and kB2 are affected by interaction with DPC micelles. Loops 2 and 5 of kB2 show the largest change on binding, suggesting that they reside at the interaction interface. By contrast, loops 2 and 3 of cO2 show the largest change on binding, indicating that the two molecules adopt different binding orientations in a micelle environment. The lack of change in chemical shift for a number of other residues fits the hypothesis that only part of the kB2 and cO2 molecules bind to the micelle, supporting the suggestion that the peptides are not buried deeply.

A sharp decrease in the translational diffusion coefficient (D_T) of cO2 during a titration with DPC further confirmed the formation of a cO2-DPC complex. A linear decrease in D_T at a D/P higher than 40:1 for cO2 can be explained by increased solvent viscosity and diffusion obstruction at a high concentration of DPC. The D_T for the cO2-DPC complex was determined to be $1.07 \times 10^{-10}\ m^2s^{-1}$ by extrapolating the data points between a D/P of 40:1 to 60:1 to zero DPC concentration to remove the effects of solvent viscosity. This is consistent with the D_T obtained for the kB1-DPC complex of $1.07 \times 10^{-10}\ m^2s^{-1}$ (27). Using the Stokes-Einstein relation, the cO2-DPC complex had a hydrodynamic radius, R_H of 26.0 Å, which is larger than the R_H of pure DPC micelle ($D_T = 1.2 \times 10^{-10}\ m^2s^{-1}$; $R_H = 23.1$ Å) (44), consistent with complex formation. It was difficult to

TABLE 1 Geometric and energetic statistics for the 20 lowest-energy structures of cO2 and micelle-bound kB2

	cO2	kB2
NMR distance and dihedral constraints		
Distance constraints		
Total NOE	347	268
Intraresidue	142	125
Interresidue	205	143
Sequential ($\|i-j\|=1$)	99	91
Medium-range ($\|i-j\|\leq 4$)	49	29
Long-range ($\|i-j\|\geq 5$)	57	23
Intermolecular	0	0
Hydrogen bonds	6	7
Total dihedral angles	18	15
ϕ	133	15
χ^1	5	0
Structure statistics		
Violations (mean and SD)		
Distance constraints (Å)	-0.13 ± 0.03	-0.15 ± 0.06
Dihedral angle constraints (°)	0 ± 0	2.61 ± 0.24
Max. dihedral angle violation (°)	0	−3.68
Max. distance constraint violation (Å)	−0.25	−0.25
Deviations from idealized geometry		
Bond lengths (Å)	0.004 ± 0.0001	0.004 ± 0.0001
Bond angles (°)	0.48 ± 0.03	0.56 ± 0.02
Impropers (°)	0.38 ± 0.04	0.5 ± 0.04
Average pairwise RMSD* (Å)		
Heavy	1.2 ± 0.22	0.89 ± 0.17
Backbone	0.35 ± 0.13	0.3 ± 0.07
Ramachandran statistics		
Most favored (%)	86.5	80.3
Allowed (%)	13.5	19.7

*Pairwise RMSD was calculated for 20 refined structures.

measure the D_T for kB2 because kB2 has limited solubility at the pH used for the titration. Although the D_T dropped upon addition of DPC, supporting the formation of a kB2-DPC complex, the low concentration at which it was necessary to record the data for kB2 resulted in unreliable data from the diffusion measurements, and thus the D_T of the kB2-DPC complex could not be estimated. At high pH, where kB2 is more soluble, significant broadening of peaks was observed in the 1D spectra in the absence of DPC when the concentration of kB2 was ~1 mM or higher, presumably because kB2 self-associates at higher concentrations, as has been shown by analytical ultracentrifugation studies (45). After the titration, addition of DPC to a concentrated sample of kB2 was found to increase the solubility of kB2 and provide 1D spectra with sharp peaks. In previous structural studies of kB2, acetonitrile was used to solubilize it (22); however, acetonitrile was not used here because it might have interfered with the binding to DPC micelles. Because kB2 interacts with DPC micelles via a hydrophobic patch on its surface (discussed below), hydrophobic interactions between different kB2 molecules may be responsible for the low solubility of kB2 in acidic aqueous solutions.

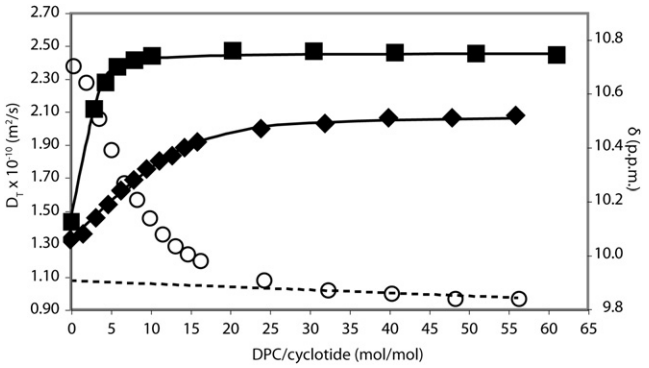

FIGURE 3 Titration of 0.5 mM kB2 and 2 mM cO2 with DPC, H_2O (10% D_2O), pH 2.8, 30°C. Chemical shift, δ, of the $H^{\varepsilon 1}$ proton of Trp^{23} and Trp^{10} of kB2 (*solid squares*) and cO2 (*solid diamonds*), respectively, are shown versus the DPC/cyclotide mole ratio. Binding curves were analyzed using the Langmuir isotherm. The diffusion coefficient, D_T, of cO2 (*open circles*) at each titration point is shown, and the dotted line shows the extrapolation of the D_T to zero detergent concentration.

Structure of micelle-bound cyclotides

NMR data were acquired for kB2 in the presence of DPC micelles and used to solve the structure of micelle-bound kB2. A comparison of the αH backbone chemical shifts with unbound kB2 (Fig. 4) suggests that there is little structural variation between the bound and unbound states. To confirm that cyclotide structures are rigid and unaffected by binding to micelles, NMR restraints were measured to determine the 3D structure. A total of 268 distance restraints, comprising 91 sequential, 52 nonsequential, and 125 intraresidue restraints, were determined from NOESY spectra, and 15 ϕ dihedral angle restraints were derived based on coupling constants from the splitting of peaks in a 1D spectrum. Slowly exchanging amides were used to derive upper limit distance restraints for six hydrogen bonds.

A backbone superimposition of the 20 lowest-energy structures obtained after energy minimization is shown in Fig. 5. Most regions of the structure are well defined, with

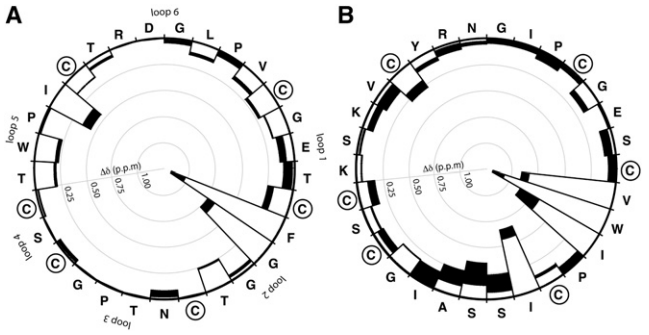

FIGURE 4 Changes in (*A*) kB2 (pH 3, 40°C) and (*B*) cO2 (pH 5, 40°C) chemical shifts, $\Delta\delta$, upon incorporation into a DPC micelle. The black and white bars for each residue denote changes in H^{α} and H^{N} chemical shifts, respectively. Cys residues are circled and the loops are numbered in the leftmost plot.

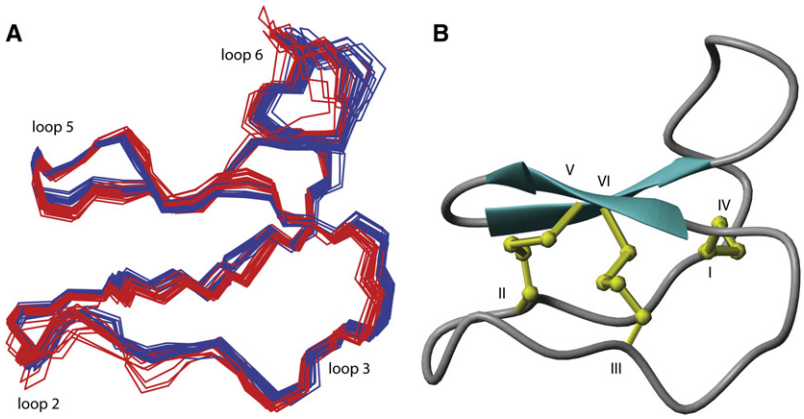

FIGURE 5 Structure of kB2 in the DPC micelle-bound state (DPC/peptide ratio 60:1, pH 5.0, 40°C). (*A*) The 20 lowest-energy structures of micelle-bound kB2 are shown in blue overlaid with the structure of unbound kB2 in red (PDB ID: 1PT4). (*B*) A ribbon representation of the structure, highlighting the disulfide knot core.

an average RMSD of 0.30 Å for the backbone atoms and 0.89 Å for the heavy atoms. The structural statistics are summarized in Table 1, and show that the restraints were fitted with minimal violations. The structure of micelle-bound kB2 is almost identical to the structure of unbound kB2, consistent with the H^{α} chemical-shift analysis presented above. This result for kB2 is consistent with the structural similarities between micelle-bound and unbound kB1 (28). An average RMSD of 0.51 Å for the backbone atoms was calculated for the combined ensemble of structures of bound and unbound kB2 (PDB ID: 1PT4). The similarity in structures between micelle-bound and unbound states confirms the rigidity of the CCK fold.

Assignment of the spectra of cO2 in DPC was challenging because the NOESY spectra were of poor quality (i.e., with many broadened peaks), even after the temperature was increased to 50°C. A comparison of the H^{α} backbone chemical shifts with unbound cO2 is shown in Fig. 4. The small differences in the H^{α} chemical shifts, combined with the expected rigidity of the cyclotides, suggest that, like kB2, the structures of cO2 in the bound and unbound states are similar, and thus a full-structure determination of micelle-bound cO2 was not attempted.

It was also difficult to study the effects of pH variation on either cO2 or kB2 bound to DPC micelles. Many of the amide signals from kB2 in the TOCSY spectra were present at pH 5 but missing at pH 3, even though the shape and number of cross-peaks in the NOESY spectra were relatively unaffected by pH variation. For cO2, several amide signals present at pH 3 in the TOCSY and NOESY spectra were missing at pH 5. Based on assignments of the spectra at a pH that gave good-quality TOCSY spectra, assignment of the NOESY spectra at the other pH was attempted. A comparison of the assigned H^{α} chemical shifts of the micelle-bound kB2 and micelle-bound cO2 at pH 3 and pH 5 revealed that the H^{α} chemical shifts did not change significantly with varying pH, suggesting that the overall backbone structure of micelle-bound kB2 and cO2 was not affected by pH. For micelle-bound kB2, three residues (Cys^{14}, Asn^{15}, and Thr^{16}) had amide chemical shifts that changed significantly (>0.1 ppm) when the pH was varied between 3 and 5 (i.e., Cys^{14} by 0.23 ppm, Asn^{15} by 2.20 ppm, and Thr^{16} by 1.62 ppm). According to the structure of micelle-bound kB2, residues Asn^{15} and Thr^{16} are involved in a hydrogen-bond network with the carboxyl of Glu^{7}, and a similar network was reported here for cO2.

Model of cyclotide-micelle complex

To determine the orientation of kB2 and cO2 relative to an associated micelle, relaxation probes that contain a nitroxide moiety, which broadens the signal of protons in its proximity, were used. When 5- and 16-doxylstearate relaxation probes are incorporated into a DPC micelle, their nitroxide moiety is preferentially located close to the surface and the center of the micelle, respectively. Specific broadening of kB2 and cO2 proton signals was monitored by comparing NOESY spectra of samples with and without paramagnetic probes (Fig. 6). The data suggest that the cyclotides were bound to the surface of the micelle, because 5-doxylstearate resulted in the attenuation of cross-peak intensities more strongly than 16-doxylstearate.

Models of the kB2-DPC and cO2-DPC complexes were built using the structures of kB2 and cO2 presented above, and data on signal attenuation induced by 5-doxylstearate. As shown in Fig. 6, the peptides interact with the micelle surface via predominantly hydrophobic interactions. For kB2, loops 1, 2, 5, and 6 reside at the interaction interface (consistent with the results for kB1 (27)), whereas a different orientation was observed for cO2, with loops 1, 2, and 3 interacting with the micelle surface. Selective attenuation of kB2 signals by Mn^{2+} confirmed the proposed kB2-DPC model. When titrated into the micellar solution, this water-soluble paramagnetic ion produced selective signal attenuation of protons not involved in the peptide-micelle interface (Supporting Material).

To determine whether the difference in membrane orientation between Möbius and bracelet cyclotides reflects their different surface properties rather than fundamentally different global folds, we undertook a quantitative RMSD

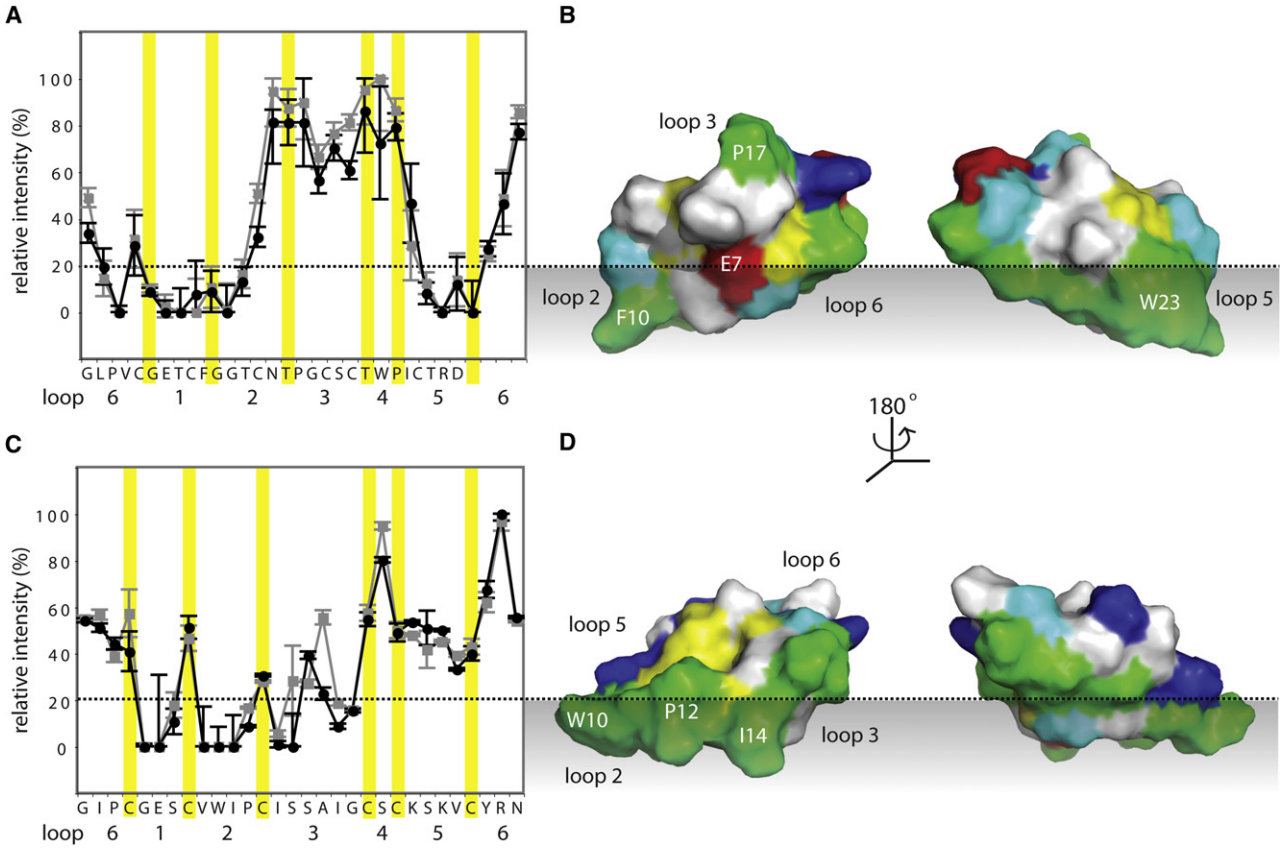

FIGURE 6 Orientation of kB2 and cO2 bound to a DPC micelle based on attenuation by doxylstearate probes. KB2 is shown in the upper row and cO2 is shown in the lower row. Either 5-doxylstearate (*black circles*) or 16-doxylstearate (*gray squares*) was added to samples containing cyclotide (1 mM, pH 3 and 40°C for kB2, pH 5 and 50°C for cO2) and DPC at a DPC/peptide ratio of 60:1. The relative cross-peaks (H^N-H^α for nonproline amino acid residues and $H^{\delta 2}$-$H^{\delta 3}$ for prolines) based on 100 ms NOESY spectra are shown on the left. To the right are the binding models based on the 5-doxylstearate data. Hydrophobic residues are colored green, negatively charged residues are red, positively charged residues are blue, Gly are cyan, polar residues are white, and Cys are yellow. A dotted line represents the 20% threshold used to determine whether residues are inside or outside of the micelle, and also schematically represents the micelle surface on the right.

comparison of all known cyclotide structures, within and between subfamilies. We found that any individual cyclotide superimposed with any other cyclotide with an RMSD in the range of 0.55–2.81 Å (Supporting Material). Although there was a slight preference for any Möbius cyclotide to be more similar to any other Möbius cyclotide than to a bracelet cyclotide, the results show that it is reasonable to regard the CCK framework as a conserved core across both subfamilies, and that the distribution of residues on the surface is the major factor in determining the different membrane interactions between the two subfamilies.

DISCUSSION

The biological mode of action of cyclotides most likely involves membrane interactions (24–27). One study (27) investigating the membrane interaction of kB1, a Möbius cyclotide, suggested that the different activity profiles for Möbius and bracelet cyclotides may be explained by different modes of peptide-membrane interaction. In the study presented here, we determined the mode of interaction of kB2 (a Möbius cyclotide) and cO2 (a bracelet cyclotide) with DPC micelles, and found that different cyclotides do indeed have clearly different modes of interaction. On the one hand, this is somewhat surprising because all cyclotides have a conserved CCK core, and it might have been assumed that they would have a common binding mode. On the other hand, it is clear from this study that it is the surface of the cyclotides, and particularly the location of a surface-exposed patch of hydrophobic residues that determine their binding mode to membrane-like surfaces. We used DPC micelles as surrogates for membranes because they are more easily studied by NMR and earlier studies have established their value as model systems (27). Surface plasmon resonance and bioactivity studies have clearly established that cyclotides functionally bind to membranes; however, the orientational information sought here could best be obtained by means of NMR studies, for which DPC micelles are the preferred model systems.

In this study, cO2 was chosen as the prototypic bracelet cyclotide because it interacts with cell membranes and liposomes, and its membrane-disrupting ability has been linked

to its cytotoxic activity (25). Additionally, it is one of the most abundant bracelet cyclotides in *V. odorata*, from which it was extracted (30,46). But before the orientation of cO2 bound to DPC micelles could be determined, the structure of cO2 needed to be solved. Structure determination by NMR spectroscopy showed the characteristic cyclic backbone and cystine knot. The secondary structure of cO2 comprises a β-hairpin centered in loop 5 (which is common among all cyclotide structures) and a helical turn in loop 3 (which has only been found in structures of bracelet cyclotides). A hydrogen-bond network involving the carboxyl of the Glu in loop 1 and two residues in loop 3, as observed in other cyclotide structures, was present in the structures of both cO2 and DPC-bound kB2. This hydrogen-bond network, which helps to stabilize the cyclotide framework (43), may explain why the Glu in loop 1 is the most highly conserved residue, apart from the cysteines, in all known cyclotides (43). The structure of cO2 further confirms that cyclotides have a conserved topology, particularly within each subfamily. The compact knotted core, which forces many of the side chains outward, means that the composition of each loop determines the surface profile and strongly influences intermolecular interactions.

Using paramagnetic attenuation of NMR signals, we identified regions of kB2 and cO2 that are responsible for peptide-DPC interactions. Loops 1, 2, 5, and 6 of kB2 formed the site of micelle binding and are responsible for hydrophobic interactions with the membrane mimic. This model of membrane binding is consistent with that proposed for kB1 (27), except for a subtle variation in loop 6, presumably because the Asp^{29} in loop 6 of kB2 is charged compared to Asn^{29} of kB2. A binding model for kB7, a Möbius cyclotide, has also been proposed (28). The model for micelle-bound kB7 is generally consistent with the micelle-bound model of kB1 and kB2, with loops 1, 2, and 5 interacting with the micelle surface. However, because kB7 contains a Lys in loop 6 instead of a Thr in position 27 of kB1 and kB2, loop 6 does not come into contact with the micelle surface in kB7. This mode of binding also helps to explain why artificially linearized cyclotides have reduced activity (47). For

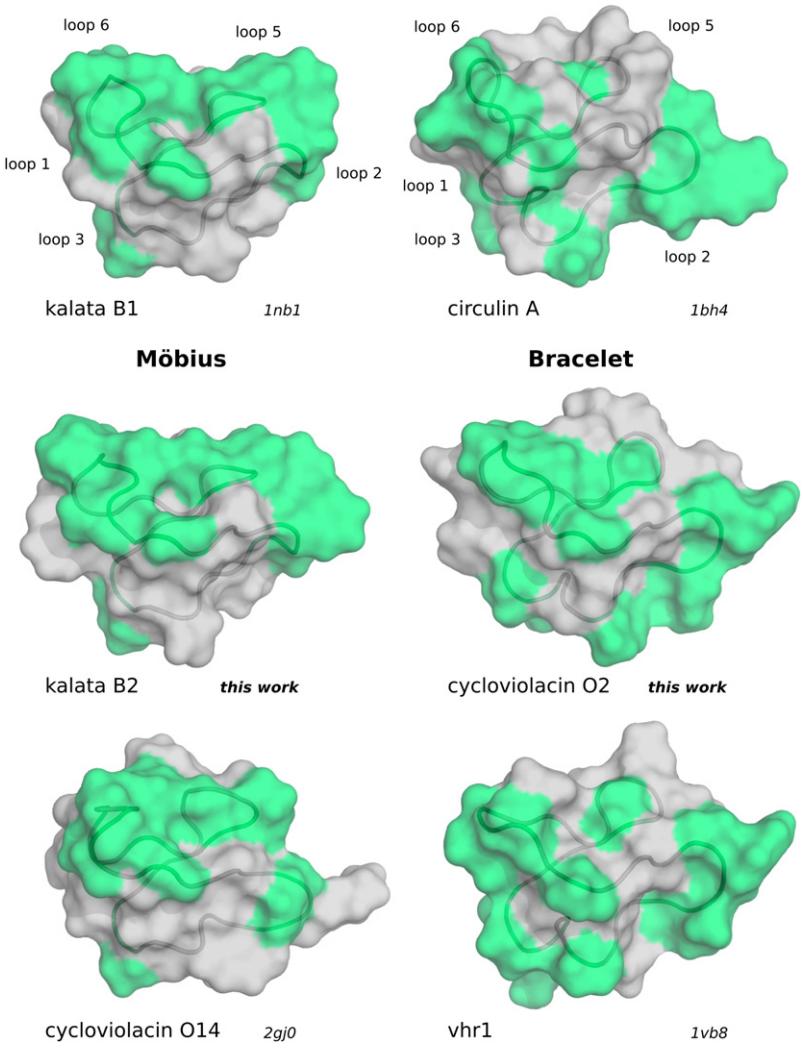

FIGURE 7 Surfaces of kB1, circulin A, kB2, cO2, cycloviolacin O14, and vhr1 are presented as representatives of the Möbius and bracelet subfamilies to show the distribution of hydrophobic residues (in *green*). The locations of the hydrophobic patches differ between bracelet and Möbius cyclotides.

example, the insecticidal activity of kB1 is abolished when loop 6 (which is involved in the binding interface) is opened to produce an acyclic analog (24). The improved membrane binding, and therefore bioactivity, of cyclic (as opposed to linear) cyclotides may explain why cyclotides have evolved, probably from a linear ancestor (48), to possess a cyclic backbone. The binding models of the three Möbius cyclotides—kB1, kB2, and kB7—suggest that hydrophobicity plays an important role in the binding of cyclotides to membrane surfaces. Because the sequences of Möbius cyclotides share a similar distribution of hydrophobic residues that cluster mainly in loop 5 and parts of loops 2 and 6, all Möbius cyclotides most likely bind in a similar orientation, with only subtle variations in the orientation, depending on the composition of amino acids in the interacting loops.

In comparison with the Möbius cyclotide kB2, cO2 from the bracelet subfamily binds to DPC micelles in a completely different orientation. This difference in the binding mode of cO2 can be attributed to the difference in surface profile compared to kB1, kB2, and kB7, in which the hydrophobic patches are located on a different face of the molecule. Instead of the hydrophobic residues being clustered in loop 5 as in Möbius cyclotides, the hydrophobic residues of bracelet cyclotides predominantly occupy loops 2 and 3 (Fig. 7). Of interest, loop 5 of the bracelet cyclotides usually contains charged residues, which would be unfavorable for interactions that are driven by hydrophobicity. This result highlights the importance of the composition of the loops (particularly the hydrophobic residues) in determining the binding orientation of cyclotides.

Several studies have suggested that the surface properties of cyclotides play an important role in determining their bioactivity. In a study relating the structure of cyclotides from *V. yedoensis* with their hemolytic and anti-HIV activity, a correlation between surface-exposed hydrophobicity and potency was established (29). An examination of the anti-HIV activity of a large number of cyclotides showed that the specific location of the hydrophobic area on the surface is important, particularly when comparing Möbius and bracelet cyclotides (49). It also showed that the hydrophobic composition of loops 5 and 6 is an important determinant of the bioactivity of Möbius cyclotides, whereas bracelet cyclotides rely on the hydrophobicity of loops 2 and 3, with the presence of charged residues also affecting the activity. The agreement between the factors that affect bioactivity and those that affect the orientation of membrane binding of cyclotides presented herein gives strong support for the role of membrane interaction in the activity of cyclotides, making this work significant in the broader scope of cyclotide function.

Although the modes of membrane binding of the Möbius and bracelet cyclotides proposed so far may cover a majority of known cyclotides based on sequence comparisons, some cyclotides with sequences that contain features from both subfamilies may have different modes of action. For example, the bracelet cyclotide kB8 (50), which does not have a *cis*-Pro in loop 5, contains a Möbius-like loop 3 that is not particularly hydrophobic and does not form a helical turn. This suggests that its mode of membrane binding may differ from that of cO2, which, like many bracelet cyclotides, has a largely hydrophobic loop 3. Unlike the Möbius cyclotides, which have a hydrophobic loop 5, kB8 has a positively charged loop 5 (from a Lys and an Arg), suggesting that the mode of binding of kB8 may also be different from the model proposed for Möbius cyclotides based on a previous study of kB1 (27) and this study of kB2. Cyclotides may have different but specific binding modes so that they can function effectively as plant defense agents by responding to different predators.

In summary, based on this characterization of how cyclotides interact with DPC micelles, we suggest that the biological activity of cyclotides is governed by their membrane interactions, which in turn are dictated by the surface profile of the cyclotides. It appears that the hydrophobic regions on the surface of cyclotides drive the initial binding to membranes, which would explain the previously observed subfamily activity characteristics (49). It will be of interest in future experiments to characterize the structure of cyclotides in lipid bilayers, which more closely mimic membrane environments.

SUPPORTING MATERIAL

Four figures are available at http://www.biophysj.org/biophysj/supplemental/S0006-3495(09)01170-9.

This work was supported by a grant from the Australian Research Council. D.J.C. is an Australian Research Council Professorial Fellow.

REFERENCES

1. Craik, D. J., N. L. Daly, T. Bond, and C. Waine. 1999. Plant cyclotides: a unique family of cyclic and knotted proteins that defines the cyclic cystine knot structural motif. *J. Mol. Biol.* 294:1327–1336.
2. Craik, D. J., N. L. Daly, J. Mulvenna, M. R. Plan, and M. Trabi. 2004. Discovery, structure and biological activities of the cyclotides. *Curr. Protein Pept. Sci.* 5:297–315.
3. Göransson, U., E. Svangard, P. Claeson, and L. Bohlin. 2004. Novel strategies for isolation and characterization of cyclotides: the discovery of bioactive macrocyclic plant polypeptides in the Violaceae. *Curr. Protein Pept. Sci.* 5:317–329.
4. Gustafson, K. R., T. C. McKee, and H. R. Bokesch. 2004. Anti-HIV cyclotides. *Curr. Protein Pept. Sci.* 5:331–340.
5. Chiche, L., A. Heitz, J. C. Gelly, J. Gracy, P. T. Chau, et al. 2004. Squash inhibitors: from structural motifs to macrocyclic knottins. *Curr. Protein Pept. Sci.* 5:341–349.
6. Wang, C. K., Q. Kaas, L. Chiche, and D. J. Craik. 2008. CyBase: a database of cyclic protein sequences and structures, with applications in protein discovery and engineering. *Nucleic Acids Res.* 36:D206–D210.
7. Saether, O., D. J. Craik, I. D. Campbell, K. Sletten, J. Juul, et al. 1995. Elucidation of the primary and three-dimensional structure of the uterotonic polypeptide kalata B1. *Biochemistry.* 34:4147–4158.
8. Colgrave, M. L., and D. J. Craik. 2004. Thermal, chemical, and enzymatic stability of the cyclotide kalata B1: the importance of the cyclic cystine knot. *Biochemistry.* 43:5965–5975.

9. Gran, L. 1973. Isolation of oxytocic peptides from *Oldenlandia affinis* by solvent extraction of tetraphenylborate complexes and chromatography on sephadex LH-20. *Lloydia.* 36:207–208.
10. Tam, J. P., Y. A. Lu, J. L. Yang, and K. W. Chiu. 1999. An unusual structural motif of antimicrobial peptides containing end-to-end macrocycle and cystine-knot disulfides. *Proc. Natl. Acad. Sci. USA.* 96:8913–8918.
11. Schöpke, T., M. I. Hasan Agha, R. Kraft, A. Otto, and K. Hiller. 1993. Hämolytisch aktive komponenten aus *Viola tricolor* L. und *Viola arvensis* Murray. *Sci. Pharm.* 61:145–153.
12. Svangard, E., U. Göransson, Z. Hocaoglu, J. Gullbo, R. Larsson, et al. 2004. Cytotoxic cyclotides from *Viola tricolor*. *J. Nat. Prod.* 67:144–147.
13. Witherup, K. M., M. J. Bogusky, P. S. Anderson, H. Ramjit, R. W. Ransom, et al. 1994. Cyclopsychotride A, a biologically active, 31-residue cyclic peptide isolated from *Psychotria longipes*. *J. Nat. Prod.* 57:1619–1625.
14. Göransson, U., M. Sjogren, E. Svangard, P. Claeson, and L. Bohlin. 2004. Reversible antifouling effect of the cyclotide cycloviolacin O2 against barnacles. *J. Nat. Prod.* 67:1287–1290.
15. Jennings, C., J. West, C. Waine, D. Craik, and M. Anderson. 2001. Biosynthesis and insecticidal properties of plant cyclotides: the cyclic knotted proteins from *Oldenlandia affinis*. *Proc. Natl. Acad. Sci. USA.* 98:10614–10619.
16. Colgrave, M. L., A. C. Kotze, D. C. Ireland, C. K. Wang, and D. J. Craik. 2008. The anthelmintic activity of the cyclotides: natural variants with enhanced activity. *ChemBioChem.* 9:1939–1945.
17. Colgrave, M. L., A. C. Kotze, Y. H. Huang, J. O'Grady, S. M. Simonsen, et al. 2008. Cyclotides: natural, circular plant peptides that possess significant activity against gastrointestinal nematode parasites of sheep. *Biochemistry.* 47:5581–5589.
18. Plan, M. R., I. Saska, A. G. Cagauan, and D. J. Craik. 2008. Backbone cyclised peptides from plants show molluscicidal activity against the rice pest *Pomacea canaliculata* (golden apple snail). *J. Agric. Food Chem.* 56:5237–5241.
19. Colgrave, M. L., A. C. Kotze, S. Kopp, J. S. McCarthy, G. T. Coleman, et al. 2009. Anthelmintic activity of cyclotides: *in vitro* studies with canine and human hookworms. *Acta Trop.* 109:163–166.
20. Craik, D. J., S. Simonsen, and N. L. Daly. 2002. The cyclotides: novel macrocyclic peptides as scaffolds in drug design. *Curr. Opin. Drug Discov. Devel.* 5:251–260.
21. Craik, D. J., M. Cemazar, C. K. Wang, and N. L. Daly. 2006. The cyclotide family of circular miniproteins: nature's combinatorial peptide template. *Biopolymers.* 84:250–266.
22. Jennings, C. V., K. J. Rosengren, N. L. Daly, M. Plan, J. Stevens, et al. 2005. Isolation, solution structure, and insecticidal activity of kalata B2, a circular protein with a twist: do Mobius strips exist in nature? *Biochemistry.* 44:851–860.
23. Plan, M. R. R., U. Göransson, R. J. Clark, N. L. Daly, M. L. Colgrave, et al. 2007. The cyclotide fingerprint in *Oldenlandia affinis*: elucidation of chemically modified, linear and novel macrocyclic peptides. *ChemBioChem.* 8:1001–1011.
24. Barbeta, B. L., A. T. Marshall, A. D. Gillon, D. J. Craik, and M. A. Anderson. 2008. Plant cyclotides disrupt epithelial cells in the midgut of lepidopteran larvae. *Proc. Natl. Acad. Sci. USA.* 105:1221–1225.
25. Svangard, E., R. Burman, S. Gunasekera, H. Lovborg, J. Gullbo, et al. 2007. Mechanism of action of cytotoxic cyclotides: cycloviolacin O2 disrupts lipid membranes. *J. Nat. Prod.* 70:643–647.
26. Kamimori, H., K. Hall, D. J. Craik, and M. I. Aguilar. 2005. Studies on the membrane interactions of the cyclotides kalata B1 and kalata B6 on model membrane systems by surface plasmon resonance. *Anal. Biochem.* 337:149–153.
27. Shenkarev, Z. O., K. D. Nadezhdin, V. A. Sobol, A. G. Sobol, L. Skjeldal, et al. 2006. Conformation and mode of membrane interaction in cyclotides: spatial structure of kalata B1 bound to a dodecylphosphocholine micelle. *FEBS J.* 273:2658–2672.
28. Shenkarev, Z. O., K. D. Nadezhdin, E. N. Lyukmanova, V. A. Sobol, L. Skjeldal, et al. 2008. Divalent cation coordination and mode of membrane interaction in cyclotides: NMR spatial structure of ternary complex Kalata B7/Mn(2+)/DPC micelle. *J. Inorg. Biochem.* 102: 1246–1256.
29. Wang, C. K., M. L. Colgrave, K. R. Gustafson, D. C. Ireland, U. Goransson, et al. 2008. Anti-HIV cyclotides from the Chinese medicinal herb *Viola yedoensis*. *J. Nat. Prod.* 71:47–52.
30. Lindholm, P., U. Göransson, S. Johansson, P. Claeson, J. Gullbo, et al. 2002. Cyclotides: a novel type of cytotoxic agents. *Mol. Cancer Ther.* 1:365–369.
31. Mulvenna, J. P., C. Wang, and D. J. Craik. 2006. CyBase: a database of cyclic protein sequence and structure. *Nucleic Acids Res.* 34:D192–D194.
32. Braunschweiler, L., and R. R. Ernst. 1983. Coherence transfer by isotropic mixing: application to proton correlation spectroscopy. *J. Magn. Reson.* 53:521–528.
33. Jeener, J., B. H. Meier, P. Bachmann, and R. R. Ernst. 1979. Investigation of exchange processes by two-dimensional NMR spectroscopy. *J. Chem. Phys.* 71:4546–4553.
34. Griesinger, C., O. W. Sørensen, and R. R. Ernst. 1987. Practical aspects of the E.COSY technique, measurement of scalar spin-spin coupling constants in peptides. *J. Magn. Reson.* 75:474–492.
35. Piotto, M., V. Saudek, and V. Sklenar. 1992. Gradient-tailored excitation for single-quantum NMR spectroscopy of aqueous solutions. *J. Biomol. NMR.* 2:661–665.
36. Goddard, T. D., and D. G. Kneller. 2005. SPARKY 3. University of California, San Francisco, CA.
37. Guntert, P., C. Mumenthaler, and K. Wüthrich. 1997. Torsion angle dynamics for NMR structure calculation with the new program DYANA. *J. Mol. Biol.* 273:283–298.
38. Brunger, A. T. 2007. Version 1.2 of the crystallography and NMR system. *Nat. Protocols.* 2:2728–2733.
39. Koradi, R., M. Billeter, and K. Wüthrich. 1996. MOLMOL: a program for display and analysis of macromolecular structures. *J. Mol. Graph.* 14:29–32.
40. Laskowski, R. A., J. A. Rullmannn, M. W. MacArthur, R. Kaptein, and J. M. Thornton. 1996. AQUA and PROCHECK-NMR: programs for checking the quality of protein structures solved by NMR. *J. Biomol. NMR.* 8:477–486.
41. Altieri, A. S., D. P. Hinton, and R. A. Byrd. 1995. Association of biomolecular systems via pulsed field gradient NMR self-diffusion measurements. *J. Am. Chem. Soc.* 117:7566–7567.
42. Dubovskii, P. V., D. V. Dementieva, E. V. Bocharov, Y. N. Utkin, and A. S. Arseniev. 2001. Membrane binding motif of the P-type cardiotoxin. *J. Mol. Biol.* 305:137–149.
43. Rosengren, K. J., N. L. Daly, M. R. Plan, C. Waine, and D. J. Craik. 2003. Twists, knots, and rings in proteins. Structural definition of the cyclotide framework. *J. Biol. Chem.* 278:8606–8616.
44. Shenkarev, Z. O., T. A. Balashova, R. G. Efremov, Z. A. Yakimenko, T. V. Ovchinnikova, et al. 2002. Spatial structure of zervamicin IIB bound to DPC micelles: implications for voltage-gating. *Biophys. J.* 82:762–771.
45. Nourse, A., M. Trabi, N. L. Daly, and D. J. Craik. 2004. A comparison of the self-association behavior of the plant cyclotides kalata B1 and kalata B2 via analytical ultracentrifugation. *J. Biol. Chem.* 279:562–570.
46. Ireland, D. C., M. L. Colgrave, and D. J. Craik. 2006. A novel suite of cyclotides from *Viola odorata*: sequence variation and the implications for structure, function and stability. *Biochem. J.* 400:1–12.
47. Daly, N. L., and D. J. Craik. 2000. Acyclic permutants of naturally occurring cyclic proteins. Characterization of cystine knot and β-sheet formation in the macrocyclic polypeptide kalata B1. *J. Biol. Chem.* 275:19068–19075.
48. Mulvenna, J. P., J. S. Mylne, R. Bharathi, R. A. Burton, N. J. Shirley, et al. 2006. Discovery of cyclotide-like protein sequences in

graminaceous crop plants: ancestral precursors of circular proteins? *Plant Cell*. 18:2134–2144.

49. Ireland, D. C., C. K. Wang, J. A. Wilson, K. R. Gustafson, and D. J. Craik. 2008. Cyclotides as natural anti-HIV agents. *Biopolymers*. 90:51–60.
50. Daly, N. L., R. J. Clark, M. R. Plan, and D. J. Craik. 2006. Kalata B8, a novel antiviral circular protein, exhibits conformational flexibility in the cystine knot motif. *Biochem. J*. 393:619–626.
51. Andersen, N. H., J. W. Neidigh, S. M. Harris, G. M. Lee, Z. Liu, et al. 1997. Extracting information from the temperature gradients of polypeptide NH chemical shifts 1997. *J. Am. Chem. Soc*. 119:8547–8561.
52. Wang, C. K., S.-H. Hu, J. L. Martin, T. Sjögren, J. Hajdu, et al. 2009. Combined X-ray and NMR analysis of the stability of the cyclotide cystine knot fold that underpins its insecticidal activity and potential use as a drug scaffold. *J. Biol. Chem*. 284:10672–10683.